SHORT-TIME ANALYSIS OF Re BEAMS STRENGTBENED WITH OR WITHOUT FRP PLATES

ANALISIS INSTANTANEO DE VIGAS DE CONCRETO ARMADO REFORZADAS CON O SIN LÁMINAS DE FIBRE REINFORCED POLYMER (FRP)

Jorge Luis Palomino Tamayo[1]

ABSTRACT

The analytical model proposed by Bazant & Oh based on compatibility of deformations and equilibrium of forces in RC cross sections is extended and presented to predict short-time deformations. Stresses and deflections in beams strengthened with 01' without FRP plates epoxy-bonded to the tension face of rectangular and T cross sections. The theory assumes concrete to have a nonzero tensile carrying capacity. A parametric study was conducted to invesugate some design parameters such as plate area. plate stiffness and strength, concrete compressive strength and steel reinforcement ratio. To this end. moment-curvat ure diagrams lI'ere generated to know the influence of such parameters in the flexural response of the section. In all cases studied, adding the plate to the cross section increases the yield and ultimate tnoment capacity substantially in sections with a low steel reinforcenient ratio in tension being this increase more significant in doubly RC sections rather than in singly ones. Furthermore, results indicate that this increased flexural capacity could vary from 1.1 *to* 3.3 *times the original strength of the section. Finally, the increase of concrete compressive strength does not increase the ultimate moment capacity significantly as it does when it is accompanied with the plate. Results show that the increased flexural capacity due to combined action could be as high as* 4 *times the original strength of the section.*

Keywords.- *Short-time, Analysis, FRP plate, Stress, Strain.*

RESUMEN

Se extiende y presenta e! *modelo analítico propuesto por Bazant &Oh basado en la compatibilidad de deformaciones y equilibrio de fuerzas en secciones de concreto armado para predecir deformaciones, esfuerzos y deflexiones instantáneas en vigas con* o *sin láminas de FRP adheridas con epóxico las secciones transversales rectangulares en forma T. La teoría supone que el concreto tiene capacidad de resistir esfuerzos en tensión. Se llevó a cabo un estudio paramétrico para investigar algunos parámetros de diseño tales como el área de la lámina, resistencia y rigidez de la lámina, resistencia a la compresión del concreto y cuantía del acero de refuerzo. Para este fin, se generaron diagramas de momento-curvatura para conocer la influencia de estos parámetros en la respuesta de flexión de la sección. En todos los casos estudiados, la adición de la lámina a la sección transversal incrementa la capacidad del momento de fluencia sustancialmente en secciones con baja cuantía de refuerzo en tensión, siendo este incremento más significativo en secciones doblemente reforzadas que en simplemente reforzadas. Además, los resultados indican que la capacidad a flexión incrementada podría variar de 1.1 a 3.3 veces la resistencia original de la sección Finalmente, .el incremento-en la resistencia a la compresión de! concreto no se incrementa la capacidad del último momento-significativamente como cuando se le acompaña con*

[1]Msc. Universidad Federal de Rio Grande do Sul - UFRGS, Centro de Mecanica Computacional –CEMACOM Porto Alegre – Brazil.

la lámina. Los resultados muestran que la capacidad de flexión es incrementada debido a la acción combinada, esta podría ser tan alta como 4 veces la resistencia original de la sección.

Palabras clave.- Instantáneo, Análisis, Lámina de FRP, Esfuerzo, Deformación.

INTRODUCTION

Most methods neglect microcracking effect of concrete in tension for simplicity in hand calculations or because it is believed that it does not produce a serious underestimation of section stiffness. The present model is an extension of the model proposed by Bazant & Oh in reference [3], which models microcraking due to strain softening considering a uniaxial stress-strain diagram and which has proved that the neglect of tensile capacity of concrete leads to a serious underestimation of stiffness in case of singly RC beams but a relatively small one in case of doubly RC beams. Because of implementation, the present model is capable of analyzing rectangular and T cross sections including a FRP plate at the tension face of the section. Furthermore, the analysis is considered to be carried out at the loading time *i*, where stress redistribution over time due to creep, shrinkage and thermal effects could be neglected. A future work wills include those effects.

Primarily, the reasons for strengthening are: (1) Durability problems due to poor or inappropriate construction material s, (2) Inadequate design or construction, (3) Aggressive environments not properly understood during the design stages, (4) Increased loading requirements due to changes or policy or use of structures, (5) Increased life-span requirements made on ageing infrastructure and (6) Exceptional or accidental loading.

RESEARCH SIGNIFICANCE

The deterioration of Peruvian infrastructure has recently spawned a variety of innovative techniques to rehabilitate structures. The use of fiber-reinforced polymer (FRP) plates for the rehabilitation and retrofit of reinforced concrete members is the most accepted practice at the present time. These FRP plates are comprised of variety of resins and fibers and are generally epoxy-bonded to the tension face of concrete beams [4]. However, these plates may be used for flexural strengthening of negative moment region of a RC beam [5].

This work describes the strength enhancement provided to the flexural capacity of RC beams by the use of CFRP (Carbon Fiber- Reinforced Polymer) plates as a particular case of a fiber-reinforced polymer. At the present study, the CFRP properties used for all computations were obtained from the technical sheet in reference [12].

CONCRETE PROPERTIES

The constitutive model for concrete in unconfined compression and tension is given in Fig. 1. For concrete in uniaxial compression, a well-known expression covering strain-softening is used [11]

$$\sigma_{c(to)} = \frac{E_{c(to)}.\varepsilon_{c(to)}}{1+\left(\frac{E_{c(to)}.\varepsilon_{cp(to)}}{\sigma_{cp(to)}}-2\right)\left(\frac{\varepsilon_{c(to)}}{\varepsilon_{cp(to)}}\right)+\left(\frac{\varepsilon_{c(to)}}{\varepsilon_{cp(to)}}\right)^2} \quad (1)$$

Several experiments have demonstrated that the value of $8_c p(w)$ could be equal to 0.002 independently of the age of concrete [9]. However, in this investigation it is assumed that the value of $8_{cp}(/o)$ is established by:

$$\varepsilon_{cp(to)} = \frac{2.\sigma_{c(to)}}{E_{c(to)}} \quad (2)$$

The corresponding value of *Ec(w)* (Mpa) for normal weight concrete is established by ACI 318 (1989) code equation [1]

$$E_{c(to)} = \begin{cases} 4730.\sqrt{\sigma_{cp(to)}} \ldots\ldots\ldots\ldots for \ldots \sigma_{cp(to)} \le 40 \\ 3300.\sqrt{\sigma_{cp(to)}} + 7000 .. for \ldots \sigma_{cp(to)} > 40 \end{cases} \quad (3)$$

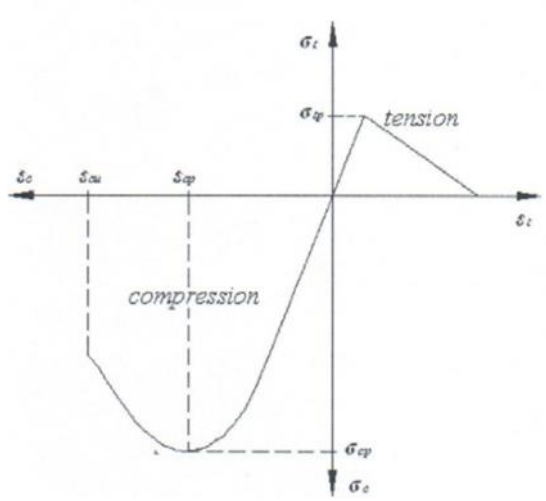

Fig. 1 *Theoretical uniaxial stress-strain curve for concrete in tension and compression.*

The bending stiffness of RC beams under service loads is considerable smaller than the stiffness calculated on the basis of uncracked cross sections.
This is because the beam contains numerous tensile cracks. Yet, at the same time, the stiffness is significantly higher than that calculated when the tensile resistance of concrete is neglected [3].

This is attributed to the fact that concrete does not crack suddenly and completely but undergoes progressive microcracking (strain softening).

For the present purposes the strain-softening behavior is modeled by a bilinear stress-strain diagram as is shown in Fig. 2 and is represented for the following equations:

$$\sigma_{t(to)} = \begin{cases} E_{c(to)}.\varepsilon_{c(to)} \ldots\ldots\ldots\ldots\ldots\ldots\ldots\ldots \varepsilon_{c(to)} \le \varepsilon_{tp(to)} \\ \sigma_{tp(to)} - \left(\varepsilon_{c(to)} - \varepsilon_{tp(to)}\right)\left(-E_{t(to)}\right) \ldots \varepsilon_{tp(to)} < \varepsilon_{c(to)} < \varepsilon_{tf(to)} \\ 0 \ldots\ldots\ldots\ldots\ldots\ldots\ldots\ldots\ldots\ldots\ldots \varepsilon_{c(to)} > \varepsilon_{tf(to)} \end{cases} \quad (4)$$

$$E_{t(to)} = \frac{-70.E_{c(to)}}{57 + 145.\sigma_{tp(to)}} \quad (5)$$

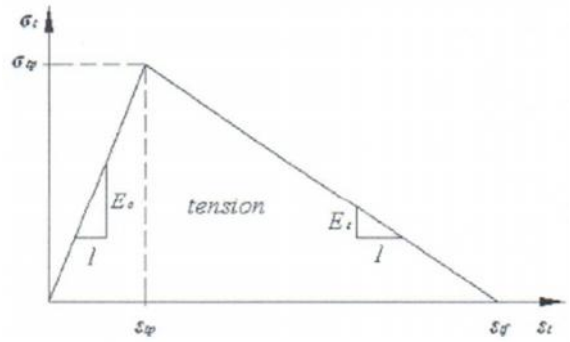

Fig. 2 *Theoretical uniaxial stress-strain curve for concrete in tension.*

CFRP PROPERTIES

The stress-strain relationship for the CFRP plate is assumed to behave linearly elastic to failure.

A wide range of composites with different mechanical properties are available in Table l.

Epoxy properties are also shown in Table 2 for adhesion between the beam and the CFRP plate.

$$\sigma_{pl} = \begin{cases} E_{pl}.\varepsilon_{pl} \ldots\ldots 0 \le \varepsilon_{pl} \le \varepsilon_{plu} \\ 0 \ldots\ldots\ldots\ldots \varepsilon_{pl} > \varepsilon_{plu} \end{cases} \quad (6)$$

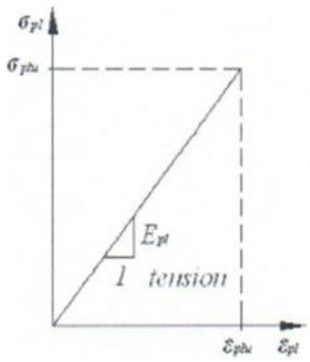

Fig. 3 *Theoretical uniaxial stress-strain curve for CFRP plate.*

STEEL PROPERTIES

The steel is assumed to have the constitutive law shown in Fig. 4 characterized by the yield stress *(J., (r..,y)* and the yield strain *e,y*

$$\sigma_{s(\varepsilon s)} = \begin{cases} \left(\frac{0.25}{34}\right)\left(\frac{\sigma_y}{\varepsilon_{sy}}\right).(\varepsilon_s + 6.\varepsilon_{sy}) - \sigma_y .. -40.\varepsilon_{sy} \le \varepsilon_s \le -6.\varepsilon_{sy} \\ -\sigma_y ..... -6.\varepsilon_{sy} \le \varepsilon_s \le -\varepsilon_{sy} \\ E_s.\varepsilon_s ..... -.\varepsilon_{sy} \le \varepsilon_s \le \varepsilon_{sy} \\ \sigma_y ..... \varepsilon_{sy} \le \varepsilon_s \le 6.\varepsilon_{sy} \\ \left(\frac{0.25}{34}\right)\left(\frac{\sigma_y}{\varepsilon_{sy}}\right).(\varepsilon_s - 6.\varepsilon_{sy}) + \sigma_y .... 6.\varepsilon_{sy} \le \varepsilon_s \le 40.\varepsilon_{sy} \end{cases} \quad (7)$$

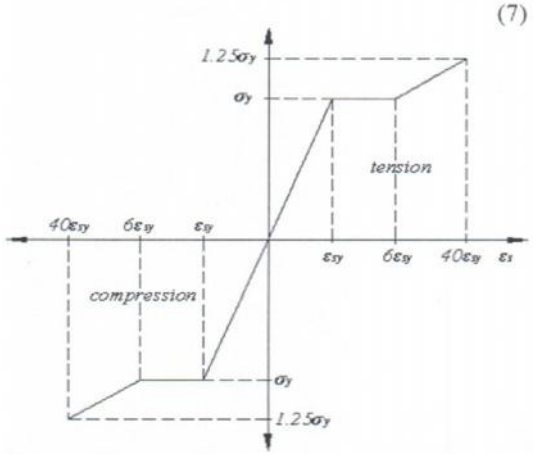

***Fig.* 4** *Theoretical stress-strain curve for steel reinforcement in compression and tension.*

Table 1. *CFRP Properties.*

Type CFRP	Width mm	Depth mm	Shear are a mm2	Tensile Strength >Mpa	Elasticity Modulus >Mpa
Sika Carbodur S					
S512	50	1.2	60	2800	165000
S612	60	1.2	72	2800	165000
S818	80	1.2	96	2800	165000
S1012	100	1.2	120	2800	165000
S1212	120	1.2	144	2800	165000
S1512	150	1.2	180	2800	165000
S614	60	1.4	84	2800	165000
S914	90	1.4	126	2800	165000
S1214	120	1.4	168	2800	165000
Sika Carbodur M					
M614	60	1.4	84	2400	210000
M914	90	1.4	126	2400	210000
M214	120	1.4	168	2400	210000
Sika Carbodur H					
H514	50	1.4	70	1300	300000

Source: *see reference [12]*

Table 2. *Epoxy properties.*

Type epoxy	Elasticity Modulus >Mpa	Bond Strength >Mpa	Shear Resistance >Mpa
Sikadur 30	12800	4	15
Sikadur 30 LP	10000	4	15
Sikadur 41	9000	4	15

Source: *see reference [12]*

ASSUMPTIONS

The followings assumptions are considered in the analysis: (1) Linear strain distribution through the full depth of the beam; (2) small deformations; (3) no shear deformations; (4) no slip between composite plate and concrete beam and (5) no slip between steel bar and concrete.

ANAL YSIS MODEL

The analysis of rectangular and T cross sections shown in Fig. 5 is now routine. The strains and stresses in the FRP plate, steel rebar and concrete as well as the curvature at midspan are calculated using an incremental deformation technique described in the following.

For the convenience of calculations, strain in the extreme fiber of concrete in compression $\varepsilon_{cm(to)}$ rather than the load is increased in specified incrernents up to concrete in cornpression reaches a strain of 0.003 or FRP plate reaches its ultirnate strength. The former allows generating mornent-curvature diagrams for different levels of load.

The strain diagram of a cross section is obtained as a function of the extreme fiber of concrete in cornpression *cCII1(IO)* where *di*,d_e and *d pl* are distances frorn the extreme fiber mentioned to the steel bars, concrete layers and the FRP plate respectively.

In case of a T cross section, *Chl(lO)* is the flange-web junction strain and $C_{III1}(IO)$ is the extreme fiber of concrete in tension.

$$\varepsilon_{s_j} = \frac{\varepsilon_{cm(to)}.(k.d - d_j)}{k.d} \qquad j = 1,2,..n \qquad (8)$$

$$\varepsilon_{c(to)} = \frac{\varepsilon_{cm(to)}.(k.d - d_c)}{k.d} \qquad (9)$$

$$\varepsilon_{pl} = \frac{\varepsilon_{cm(to)}.(k.d - d_{pl})}{k.d} \qquad (10)$$

$$\varepsilon_{h1(to)} = \frac{\varepsilon_{cm(to)}.(k.d - h_1)}{k.d} \qquad (11)$$

$$\varepsilon_{tm(to)} = \frac{\varepsilon_{cm(to)}.(k.d - h)}{k.d} \qquad (12)$$

Next, stresses in the steel bars, concrete layers and the FRP plate follow frorn the constitute laws of the rnaterials shown above. The resultant forces of concrete in compression and tension depends upon the shape of the section and the positions of the neutral axis.

The following equations are applied for a T cross section reinforced by various steel bars near the bottorn and top fibers of the section. Consider the case when *kd* :::; *h,* , the web area and part of the flange are a are in tension. Therefore, it is established for concrete two tension forces for representing stresses acting in these areas denoted as e" and e_{l2} respectively plus an additional cornpression force $e_{c'}$ for the part of the flange area in compression.

For *k.d s; h*$_l$

$$C_{c1(to)} = \alpha_1.\sigma_{cp(to)}.b.k.d \qquad (13)$$

$$C_{t1(to)} = \alpha_{t1}.\sigma_{tp(to)}.b.(k.d - h_1) \qquad (14)$$

$$C_{t2(to)} = \alpha_{t2}.\sigma_{tp(to)}.b_1.(h - h_1) \qquad (15)$$

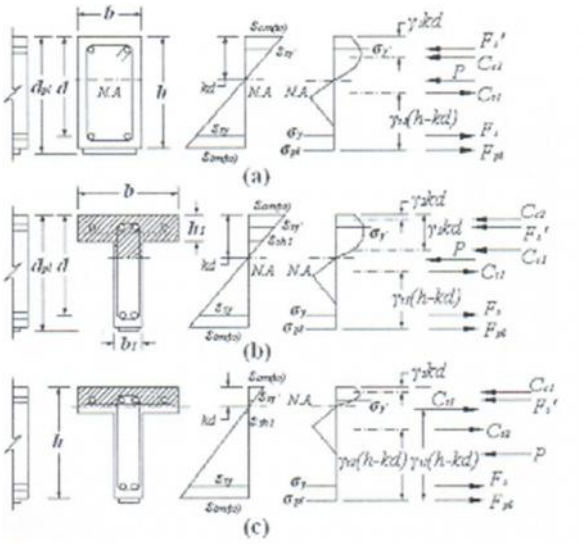

Fig. 5 Stress and strain distributions in the cross section of beams

$$\alpha_1 = \frac{\int_0^{\varepsilon_{cm(to)}} \sigma_{c(to)}.d\varepsilon_c}{\sigma_{cp(to)}.\varepsilon_{cm(to)}} \qquad (16)$$

$$\alpha_{t1} = \frac{\int_0^{\varepsilon_{h1(to)}} \sigma_{t(to)}.d\varepsilon_c}{\sigma_{tp(to)}.\varepsilon_{tm(to)}} \qquad (17)$$

$$\alpha_{t2} = \frac{\int_{\varepsilon_{h1(to)}}^{\varepsilon_{tm(to)}} \sigma_{t(to)}.d\varepsilon_c}{\sigma_{tp(to)}.\varepsilon_{tm(to)}} \qquad (18)$$

$$\gamma_1 = 1 - \frac{\int_0^{\varepsilon_{cm(to)}} \sigma_{c(to)}.\varepsilon_{c(to)}.d\varepsilon_c}{\varepsilon_{cm(to)}.\int_0^{\varepsilon_{cm(to)}} \sigma_{c(to)}.d\varepsilon_c} \qquad (19)$$

$$\gamma_{t1} = 1 - \frac{\int_0^{\varepsilon_{h1(to)}} \sigma_{t(to)}.\varepsilon_{c(to)}.d\varepsilon_c}{\varepsilon_{tm(to)}.\int_0^{\varepsilon_{h1(to)}} \sigma_{t(to)}.d\varepsilon_c} \qquad (20)$$

$$\gamma_{t2} = 1 - \frac{\int_{0}^{\varepsilon_{tm(to)}} \sigma_{s(to)} \cdot \varepsilon_{c(to)} \cdot d\varepsilon_c}{\varepsilon_{tm(to)} \cdot \int_{\varepsilon_{h1(to)}}^{\varepsilon_{tm(to)}} \sigma_{s(to)} \cdot d\varepsilon_c} \quad (21)$$

$$N_{(\varepsilon_{cm(to)} k.d_{(to)})} = C_{c1(to)} + C_{t1(to)} + C_{t2(to)} + \sum_{j=1}^{n} \sigma_{s(ss)} \cdot A_{sj} + \sigma_{pl} \cdot A_{pl} + P = 0 \quad (22)$$

$$M = C_{c1(to)} \cdot \left(\frac{h}{2} - \gamma_1 \cdot k.d \right) + C_{t1(to)} \cdot \left(\frac{h}{2} - \gamma_{t1} \cdot (h - k.d) \right) + C_{t2(to)} \cdot \left(\frac{h}{2} - \gamma_{t2} \cdot (h - k.d) \right) + \sum_{j=1}^{n} \sigma_{s(ss)} \cdot A_{s_j} \cdot \left(\frac{h}{2} - d_j \right) + \sigma_{pl} \cdot A_{pl} \cdot \left(\frac{h}{2} - d_{pl} \right) \quad (23)$$

When $k.d > h.$, the flange area and part of the web area are in cornpression.

Therefore, it is established for concrete two compression forces for representing the stresses acting in these areas denoted as C_{cJ} and C_{c2} respectively plus an additional tension force C, J for the part of the web area in tension.

For $k.d > h$,

$$C_{c1(to)} = \alpha_1 \cdot \sigma_{cp(to)} \cdot b_1 \cdot (k.d - h_i) \quad (24)$$

$$C_{c2(to)} = \alpha_2 \cdot \sigma_{cp(to)} \cdot b \cdot (k.d) \quad (25)$$

$$C_{t1(to)} = \alpha_{t1} \cdot \sigma_{tp(to)} \cdot b_i \cdot (k.d - h) \quad (26)$$

$$\alpha_1 = \frac{\int_{0}^{\varepsilon_{h1(to)}} \sigma_{c(to)} \cdot d\varepsilon_c}{\sigma_{cp(to)} \cdot \varepsilon_{cm(to)}} \quad (27)$$

$$\alpha_2 = \frac{\int_{\varepsilon_{h1(to)}}^{\varepsilon_{cm(to)}} \sigma_{c(to)} \cdot d\varepsilon_c}{\sigma_{cp(to)} \cdot \varepsilon_{cm(to)}} \quad (28)$$

$$\alpha_{t1} = \frac{\int_{0}^{\varepsilon_{tm(to)}} \sigma_{s(to)} \cdot d\varepsilon_c}{\sigma_{tp(to)} \cdot \varepsilon_{tm(to)}} \quad (29)$$

$$\gamma_1 = 1 - \frac{\int_{0}^{\varepsilon_{h1(to)}} \sigma_{c(to)} \cdot \varepsilon_{c(to)} \cdot d\varepsilon_c}{\varepsilon_{cm(to)} \cdot \int_{0}^{\varepsilon_{h1(to)}} \sigma_{c(to)} \cdot d\varepsilon_c} \quad (30)$$

$$\gamma_2 = 1 - \frac{\int_{\varepsilon_{h1(to)}}^{\varepsilon_{cm(to)}} \sigma_{c(to)} \cdot \varepsilon_{c(to)} \cdot d\varepsilon_c}{\varepsilon_{cm(to)} \cdot \int_{\varepsilon_{h1(to)}}^{\varepsilon_{cm(to)}} \sigma_{c(to)} \cdot d\varepsilon_c} \quad (31)$$

$$\gamma_{t1} = 1 - \frac{\int_{0}^{\varepsilon_{tm(to)}} \sigma_{s(to)} \cdot \varepsilon_{c(to)} \cdot d\varepsilon_c}{\varepsilon_{tm(to)} \cdot \int_{0}^{\varepsilon_{tm(to)}} \sigma_{s(to)} \cdot d\varepsilon_c} \quad (32)$$

Now the force and moment equilibrium conditions may be written as:

$$N_{(\varepsilon_{cm(to)} k.d_{(to)})} = C_{c1(to)} + C_{c2(to)} + C_{t1(to)} + \sum_{j=1}^{n} \sigma_{s(ss)} \cdot A_{sj} + \sigma_{pl} \cdot A_{pl} + P = 0 \quad (33)$$

$$M = C_{c1(to)} \cdot \left(\frac{h}{2} - \gamma_1 \cdot k.d \right) + C_{c2(to)} \cdot \left(\frac{h}{2} - \gamma_2 \cdot k.d \right) + C_{t1(to)} \cdot \left(\frac{h}{2} - \gamma_{t1} \cdot (h - k.d) \right) + \sum_{j=1}^{n} \sigma_{s(ss)} \cdot A_{s_j} \cdot \left(\frac{h}{2} - d_j \right) + \sigma_{pl} \cdot A_{pl} \cdot \left(\frac{h}{2} - d_{pl} \right) \quad (34)$$

The previous equations are also applicable for a rectangular section by setting $b = b_i$ and $h = h_i$. Finally, the section curvature is taken as:

$$\psi_{(to)} = \frac{\varepsilon_{cm(to)}}{k.d} \quad (35)$$

According to the principIe of virtual work, deflections may be calculated as [3].

$$\delta_{(to)} = \int \psi_{(to)} \cdot M \, dx \quad (36)$$

In which M = bending moment distribution corresponding to a unit load in the sense of deflection δ.

NUMERICAL ANAL YSIS

A computer program ARCS (Analysis of Reinforced Concrete Sections) was developed to carry out all computations. The Newton-Raphson method was used to solve equations given by the equilibrium conditions.

A rapid convergence is reported to solve equations (22) and (33) when $C_{Cm}(lO)$ is known. Numerical examples are verified with ARCS in order to establish agreement. For instance, for the sake of illustration, example 1 in reference [3] is recreated including the model proposed by El-Mihilrny and Tedesco (E&T) developed for the analysis of rectangular beams strengthened with FRP plates for additional comparison. In this example, a simply supported beam subjected to a concentrated load at midspan is analyzed.

The design parameters for the singly reinforced beam are: b = 30 cm (12 in), h = 60 cm (24 in), A_s = 31.25 cm2 (5 in2), d = 50 cm (20 in), $f_c^{'} = \sigma_{cp(to)}$ = 24.82 Mpa (3600 psi), $f_1^{'} = \sigma_{tp(to)}$ = 3.10 Mpa (450 psi), $Ee(to)$ = 23580.90 Mpa (3.42.10^6 psi), $\sigma_{s(\varepsilon sy)}$ = 275.80 Mpa (40000 psi), E_s=199955.00 Mpa (29.10^6 psi) and L =4.50 m (180 in)

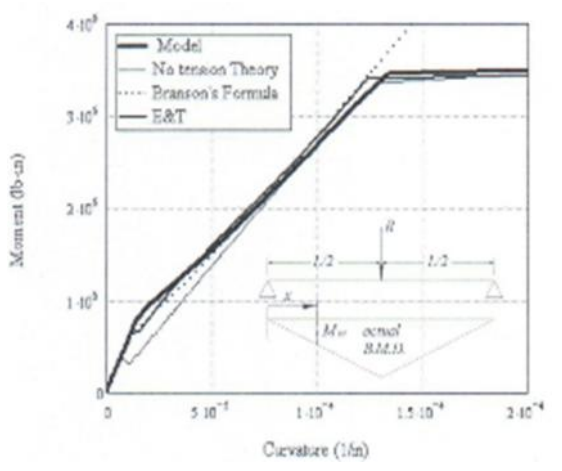

***Fig.* 6** *Moment-curvature diagram for comparison of the present model, no-tension theory, Branson 's Formula and EI- Mihilmy and Tedesco Model.*

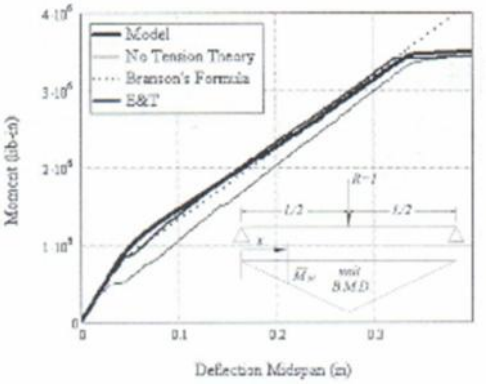

***Fig.* 7** *Moment-deflection diagram for comparison of the present model, no-tension theory, Branson 's Formula and EI- Mihilmy and Tedesco Model*

Figs. 6 and 7 are kept in British units for easy comparison with Figs. 3 and 4 in reference [3]. In fact, figures show good reement between the present model and the EI-Mihilmy-Tedesco model which rnodifies Branson's formula to predict the region beyond first yielding of the steel bar and which has been intended to include a FRP plate in the sectional analysis. Otherwise, the present model including a FRP late will be validated in theory by comparison with the EI-Mihilmy and Tedesco model which has proved to predict results with an acceptable percentage of error in the generation of moment-curvature and deflections diagrams for beams. For instance, the last example is computed adding a CFRP plate of the type S in the analysis with various plate area to gross concrete area ratios: Apl / $b.h$ = 0.25%, 0.50%, 0.75% and 1.5%.

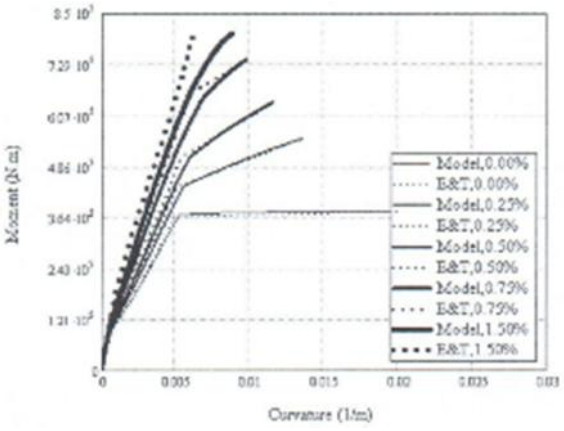

***Fig.* 8** *Moment-curvature diagram for beam of example* 1 *including the composite plate* S.

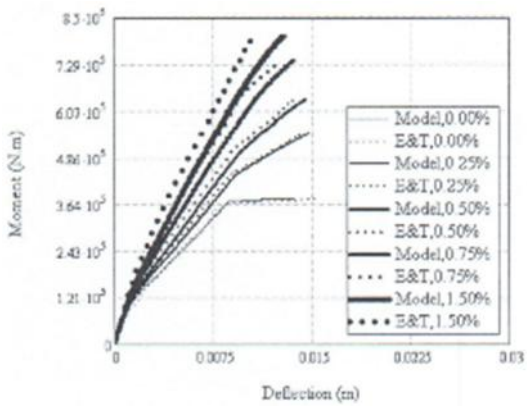

***Fig.* 9** *Moment-deflection diagram for beam of example* 1 *including the composite plate* S.

As can be seen from Figs. 8 and 9, there is good agreement between both models despite that E&T model is an approximate method of estimation. Nevertheless, more discrepancy is appreciated as plate area increases although ultimate moment capacity is almost the same for all curves. Having validated the model for the analysis of rectangular cross sections strengthened with or without FRP plates, a parametric study was carried out to investigate some design parameters.

PARAMETRIC STUDY

Moment-curvature diagrams for cross sections of rectangular and T shape are plotted using the present model for investigating various design parameters such as steel reinforcement ratio, plate area, plate ultimate strength and stiffness, and concrete compressive strength.

In the diagrams, R and T stand for rectangular and T cross sections respectively; the second column stand s for the type of CFRP plate chosen from table 1, S indicates *Epl* = 165000 Mpa, *Fpl* = 2800 Mpa, H indicates *Epl* =300000 Mpa, *Fpl* = 1300 Mpa, the third column stand s for compressive strength of concrete *(Jcp(to)* = 20.7 MPa, 27.6 Mpa, 4].4 Mpa, and the fourth column stands for plate area to gross concrete area ratio *Apl* / *bh* = 0.00%, 0.25%, 0.50% and 1.50%. In addition, properties of steel bar are taken as: yield stress (J,(€,y) = 414 Mpa, modulus of elasticity *Es* = 200000 MPa, tensile strength of concrete is taken as *(Jtp(to) = 0.1,(J cp(to)'* Each curve is ended when concrete strain in compression reaches a strain of 0.003 or composite plate reaches its ultimate strength.

***Table* 3**. *Sections for the analysis.*

Section	*p* %	*p'* %	*b* m	*h* m	*bl* m	*hl* m
Rl	3.750	2.500	0.30	0.60		
R2	3.750	1.250	0.30	0.60		
R3	3.750	0.000	0.30	0.60		
R4	2.500	1.250	0.30	0.60		
R5	2.500	0.000	0.30	0.60		
R6	1.250	0.625	0.30	0.60		
R7	1.250	0.000	0.30	0.60		
R8	0.625	0.000	0.30	0.60		
TI	0.500	0.310	0.61	0.455	0.205	0.075
T2	1.500	0.310	0.61	0.455	0.205	0.075

Source: see reference [8], [13]

RECTANGULAR BEAMS

Fig. 10 shows the moment-curvature diagrams for cross sections in Table 3 without plate. Importantly, it is noted that ductility of singly Re sections decreases as steel reinforcement ratio in tension increases and the presence of steel reinforcement ratio in compression increases ductility significantly [9].

Furthermore, the following diagrams shown that adding the composite plate to the section increases the yield and ultimate moment capacity significantly and the area under the curves does not changed appreciably although ductility decreases. In Figs. 13, 15, 17 and 1/8 are shown that the gain in the yield and ultimate moment capacity compared to the original strength of the section is not significant as the steel reinforcement ratio in tension increases.

As a result, the use of the composite plate does not increase the ultimate moment capacity substantially as it does when a cross section has a relative low steel reinforcement ratio in tension. The maximum increased flexural capacity could be as high as 3.3 times the original strength of the section as is shown in Fig. 18.

On the other hand, Figs. 11, 12, l3 and Figs. 14 and 15 show that steel reinforcement ratio in compression increases the yield and ultimate

moment capacity up to 60% for section R4. In Figs. 19,20,21,25,26 and 27, the effect of an increase in the compressive strength of concrete in combination with the addition ofthe plate increases the ultimate moment capacity beyond those curves plotted in Figs. 13, 15, 18, and Figs. 22, 23, 24 where the concrete compressive strength is taken as the half. From Figs. 22 to 27, the type of plate has been changed to the type H which has the lowest tensile strength according to Table l.

Because of its constitutive law, the type of plate H exhibits a higher resistance for the same strain compared to other composite plate because of its higher elasticity modulus despite that its rupture strain is sooner.

This is the reason to explain the behaviour of curves in figures from 22 to 27 which display a little larger resistance (becoming the plate H stiffer) and not a smaller one as it could have been expected due to its lower ultimate strength. Also, Fig. 27 shows that the maximum increased flexural capacity could be as high as 4 times the original strength of the section, for instance.

A clarification should be established for Figs. 24 and 27, where the curves at the end follow a straight line with a negative slope up to the original resistance curves for keeping equilibrium of internal forces because of failure of the plate has taken place before concrete crushing. Fig. 28 shows the relationship between the ultimate moment capacity of the sections R3, R5, R7 and R8 and the steel reinforcement ratio in tension for four plate areas to gross concrete area, *Apl* / *bh* = 0.00%, 0.25%, 0.50% and 1.50%. As can be seen, the ultimate moment capacity increases as steel reinforcement ratio in tension and plate area to gross concrete area ratio increases.

However, the rate of increase decreases as the plate area to gross concrete are a increases what can be visualized by the decrease of the slopes.

Finally, Fig. 29 shows the relationship between the ultimate moment capacity and the plate area to gross concrete area ratio for section R8 which has the lowest steel reinforcement ratio in tension. The curves were generated for both types of plate S and H and for four plate are a to gross concrete are a ratios *Apl* / *bh* = 0.00%, 0.25%, 0.50% and 1.50%.

As can be seen, the ultimate moment capacity increases as the plate area to gross concrete are a increases. However, the rate of increase in the ultimate moment capacity decreases as the plate area increases.

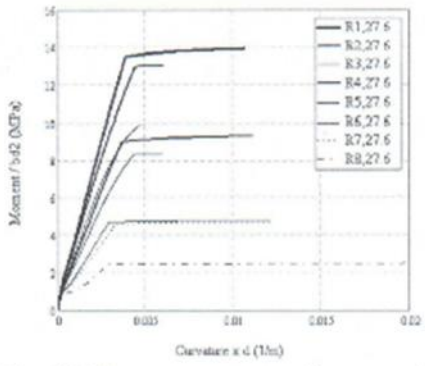

Fig. 10 Moment-curvature diagram for sections from Table 3

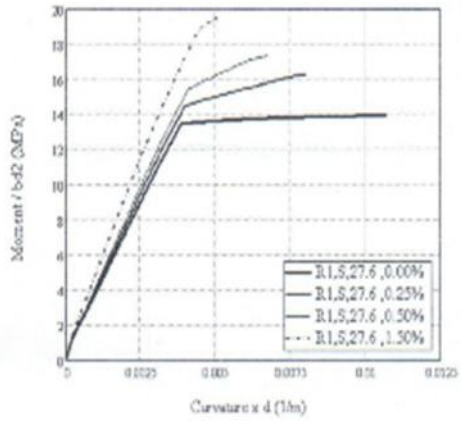

Fig. 11 Moment-curvature diagram (section R1)

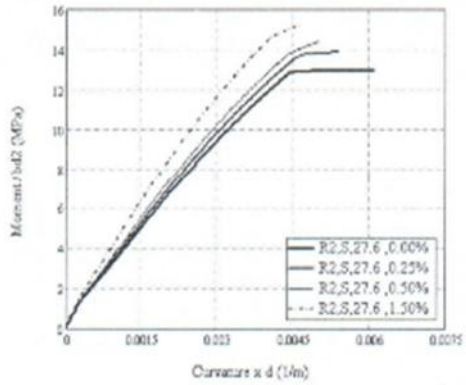

Fig. 12 Moment-curvature diagram (section R2)

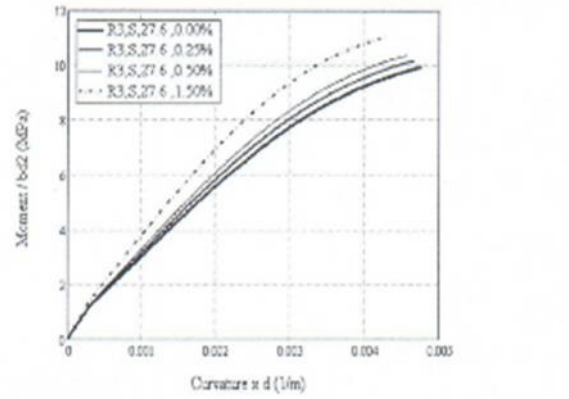

Fig. 13 Moment-curvature diagram (section R3)

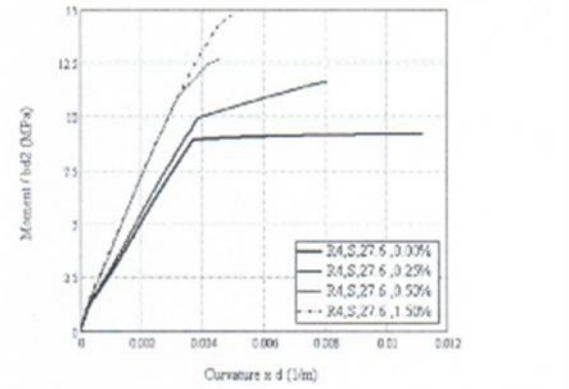

Fig. 14 Moment-curvature diagram (section R4)

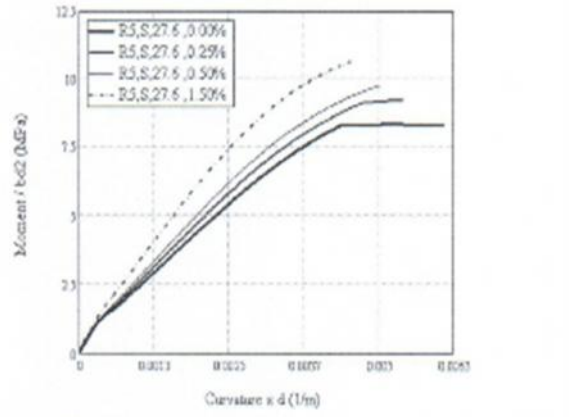

Fig. 15 Moment-curvature diagram (section R5)

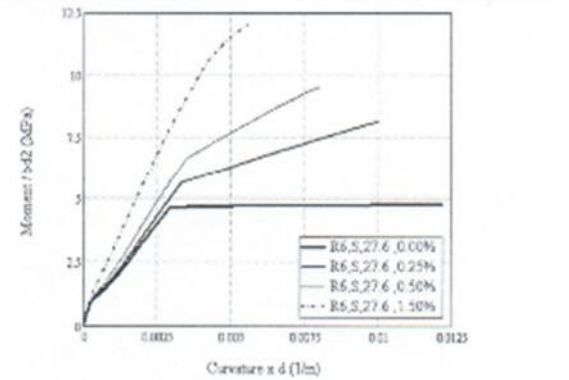

Fig. 16 Moment-curvature diagram (section R6)

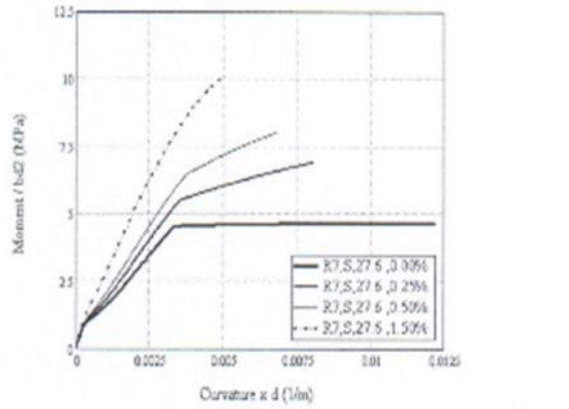

Fig. 17 Moment-curvature diagram (section R7)

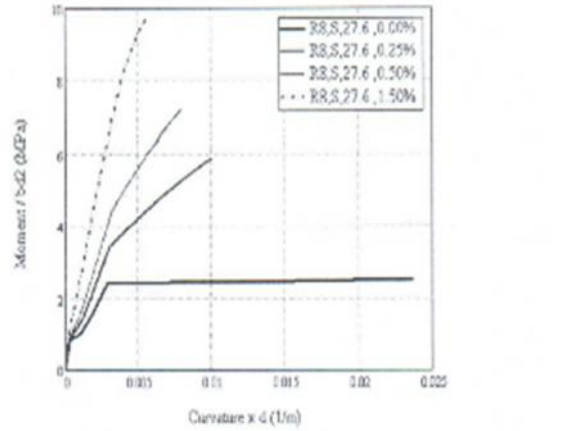

Fig. 18 Moment-curvature diagram (section R8)

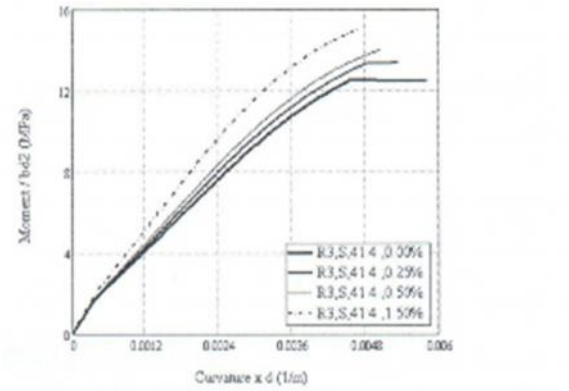

Fig. 19 Moment-curvature diagram (section R3)

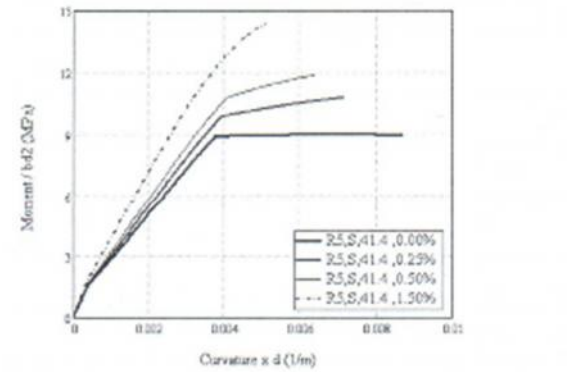

Fig. 20 Moment-curvature diagram (section R5)

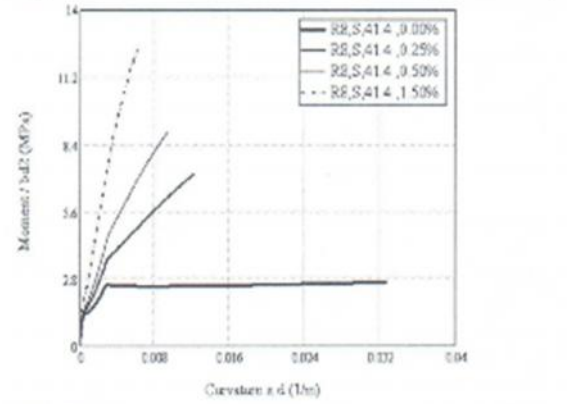

Fig. 21 Moment-curvature diagram (section R8)

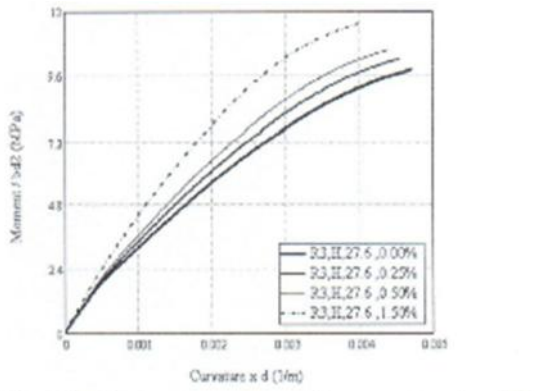

Fig. 22 Moment-curvature diagram (section R3)

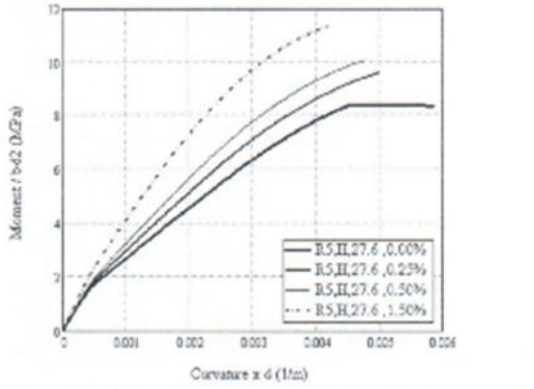

Fig. 23 Moment-curvature diagram (section R5)

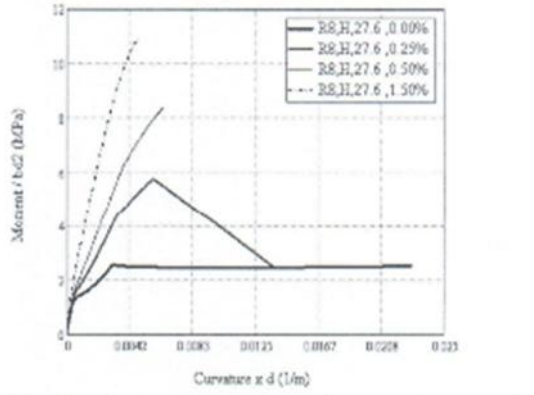

Fig. 24 Moment-curvature diagram (section R8)

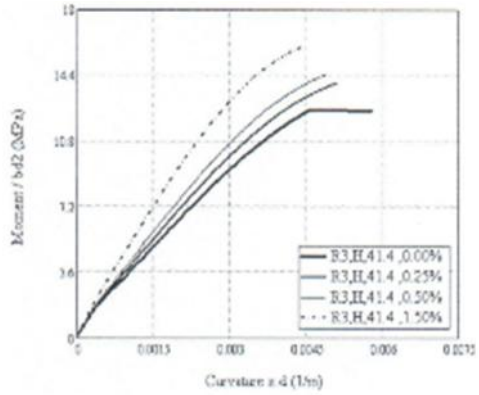

Fig. 25 Moment-curvature diagram (section R3)

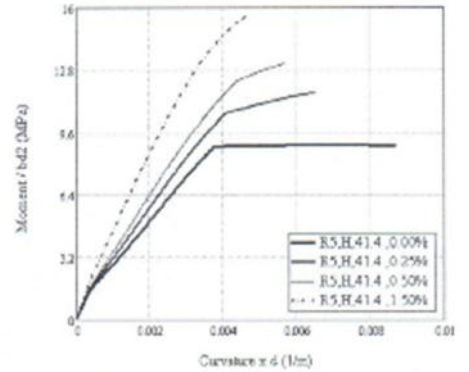

Fig. 26 Moment-curvature diagram (section R5)

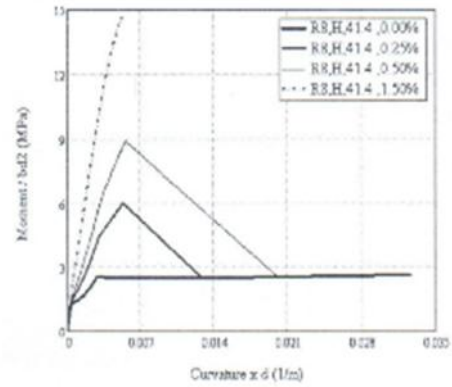

Fig. 27 Moment-curvature diagram (section R8)

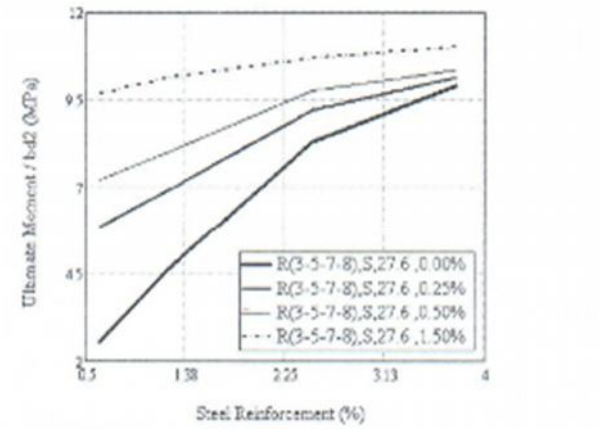

Fig. 28 Ultimate Moment versus Steel Ratio

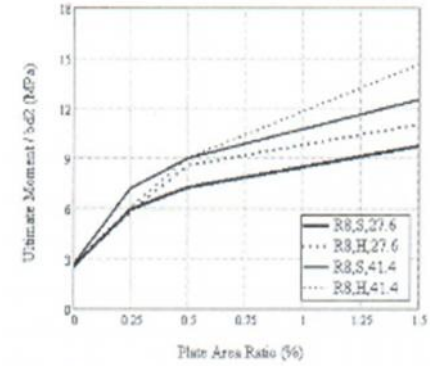

Fig. 29 Ultimate Moment versus Plate Area to Gross Concrete Area

T BEAMS

The moment-curvature diagrams for cross sections of T shape are plotted considering the steel reinforcement ratio established according to Table 3, In this section, the concrete compression strength was considered to be equal to *O'Cp(lo)* = 20,7 MPa, four different ratios of plate area to gross concrete area are taken *Apt* / *bh* = 0.00%, 0,25%, 0,50% and 1.50%, the chosen composite plate was the type S, other design variables are kept similar to the rectangular case.

For all diagrams plotted, *b* = width of the web and the decreasing straight line which implies FRP failure has not been drawn as it was done previously just for arrangement. In Fig. 30, the moment-curvature diagram for section TI is shown. As can be seen, adding the composite plate to the tension face of the section increases the yield and the ultimate moment capacity and reduces the curvature in failure, The failure in this case was achieved because of the composite plate

reaches its ultimate strength in tension except for the curve with *Apt* / *bh* = 1,50% where crushing of concrete occurs firstly.

The reason for FRP failure is attributed to the fact that the neutral axis was located close to the top of the flange are a producing a longer distance between the neutral axis and the composite plate area.

This fact results in larger strains in the composite plate than in the extreme fiber of concrete in cornpression.

Fig, 31 shows the moment-curvature diagram for section T2 with the same design parameters used to plot Fig. 30 except for a higher steel reinforcement ratio in tension equal to p = 1.5%. Here, the main mode of failure is because of crushing of concrete in compression at strain of 0,003, except for the curve with *Apl* / *bh* = 0,25% where the composite plate reaches its ultimate strength firstly, additionally, adding the composite plate to the tension face of the section increases the yield and ultimate moment capacity in a similar manner to the previous case although in a smaller amount due to the current higher steel reinforcement ratio.

In conclusion, it is established that the increased flexural capacity for the sections TI and T2 is increased in 2.5 and 0.4 times the original strength of the sections respectively.

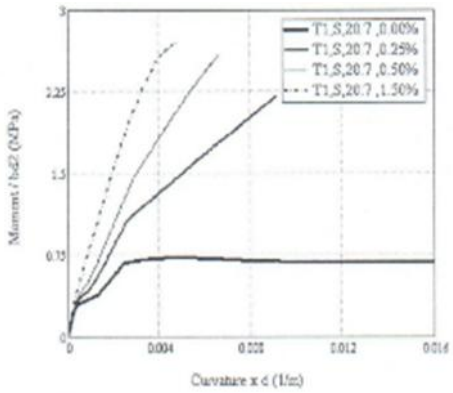

Fig. 30 Moment versus Curvature (section T1)

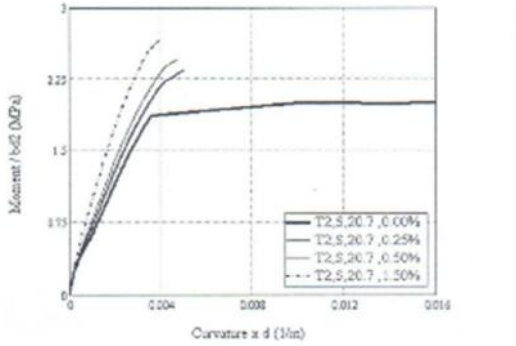

Fig. 31 Moment versus Curvature (section T2)

CONCLUSIONS

The analytical model presented by Bazant & Oh in reference [3] is extended for analyzing cross sections of rectangular and shape strengthened with or without FRP plates at the tension face for generating moment-curvature relationships. Results of the present study have been compared with other results from references such as [3], [4] and [13], which have correlated well with experimental data. It should be emphasized again that in the case of RC beams without plates, the neglect of tensile capacity of concrete leads to a serious underestimation of stiffness in case of singly RC beams, primarily, the contribution of the present study is the parametric investigation conducted for the analysis of RC sections strengthened with CFRP plates. Adding the composite plate to the tension face of a Re section increases the yield and ultimate moment capacity and reduces the curvature in failure for all sections studied. The increased flexural capacity varies from 1.1 to 3.3 times the original strength of the section depending upon the amount of steel reinforcement ratio of the section. However, the increase decreases as the steel reinforcement ratio in tension increases what indicates that this technique will be used when there is a lack of sufficient reinforcement in the section.

Also, increasing the concrete compressive strength does not appreciably increase the yield and ultimate moment capacity by itself. Nevertheless, this increase is more significant in RC cross sections with a higher steel reinforcement ratio in tension. As a result, it is concluded that the increase in the compressive concrete strength combined with the composite plate increase the original strength of a rectangular section up to 4 times.

ACKNOWLEDGEMENTS

The author gratefully acknowledges the financial support provided in part by Mr. Máximo Palomino Perez. Karena Quiroz Jimenez is thanked for her constant assistance,

Notation

A_{pl} : FRP cross-sectional area.
A_s : Reinforcing steel cross-sectional area.
b : T cross section flange width.
b_1 : Beam cross section width.
$C_{CI(to)}$: Compressive force at t_o,
$C_{c2(to)}$: Compressive force at t_o.
$C_{tl(to)}$: Tensile force at t_o,
$C_{t2(to)}$: Tensile force at t_o,
d : Depth ofthe section.
d_c : Distance from the extreme compression fiber of concrete to any concrete fiber.
d_j : Distance from the extreme compression fiber of concrete to steel reinforcement.
d_{pl} : Distance from the extreme compression fiber of concrete to FRP plate.
$E_{c(to)}$: Concrete modulus of elasticity at t_o
E_{pl} : FRP modulus of elasticity.
E_s : Reinforcing steel modulus of elasticity.
$E_{t(to)}$: Tangent strain-softening modulus of concrete at t_o.
F_s : Steel force in tension.
F_s' : Steel force in compression.
F_{pl} : FRP force.
h : Height of beam cross section.
h_1 : T cross section flange thickness.
L : Length o the beam.
M : Resultant moment of sectional stresses
$\bar{M}$: Resultant moment due to a unit load.
N : Resultant axial force of sectional stresses.
P : Applied axial force.
R : Applied force at midspan.
t_o : Loading time.
x : Distance from left support ofthe beam.
α_1 : Average stress factor for concrete m compression.
α_2 : Average stress factor for concrete m compression.
α_{tl} : Average stress factor for concrete m tension.
α_{t2} : A verage stress factor for concrete m tension.
$\delta_{(to)}$: Deflection at t_o
CC(IO): Concrete strain at *lo*
Ccp(tn): Strain at compression peak stress at *lo*
Chl(lo) : Strain at the flange-web junction.
C *pl* : FRP tensile strain.
C *plu* : FRP ultimate tensile strain.
col) : Steel strain at fiber *j* .
c_{sy} : Steel yield strain.
cl/(IO) : Ultimate tensile strain when tensile stress is reduced to zero at *lo.*
Clp(IO : Strain at peak tensi le stress at *lo.*
l//(tn) : Sectional curvature at *lo·*
YI : Dimensionless factor which defines position of compression concrete force.
Y2 :*Dimensionless factor which defines position of compression concrete force.*
Yt/ *Dimensionless factor which defines position oftensile concrete force*
YI2 :*Dimensionless factor which defines position oftensile concrete force*
k :*Dimensionless factor which defines neutral axis depth.*
p : *Steel reinforcement ratio in tension*
p' : *Steel reinforcement ratio in compression.*
(fe(lo) : *Concrete compression stress atto·*
(fCp(IO): Peak concrete compression stress atto·

: FRP tensile stress
: Steel stress at fiber j.
: Steel yield stress.
: Concrete tensi le stress at to .
: Peak concrete tensile stress at to.

Subscripts

e : Concrete.
j : *j¡h* steel layer.
pl : Composite plate.
s : Steel.
t : Tension.

Superscripts

‘ : Compression

REFERENCES

1. **Abushoglin, F.**, "Cornputer-Aid Nonlinear Analysis of Simple Beams and One Way Slabs Reinforced by FRP and/or Steel Bars", Master thesis, Carleton University, Ottawa, 1997.
2. **Alwis, W. A. M.,** "Stress redistribution in *RlC* beams and columns", Sixth lnternational Conference on Creep, Durability Mechanics

of Concrete and Other Quasi - Brittle Materials (CONCREEP-6), papers, pp. 803-808, Massachusetts, 2001.

3. **Bazant, Z. P., Oh, B. H.,** "Deformation of Progressively Cracking Reinforced Concrete Beams," ACI Journal; *Proceedings* V.81, N° 3, pp. 268-278, 1984.
4. **EI-Mihilrny, M. T., Tedesco, J. W.**, "Deflection of Reinforced Concrete Beams Strengthened with Fiber-Reinforced Polymer (FRP) Plates", ACI Structural Journal; *Proceedings* V.97, N° 5, pp. 679-688, 2000.
5. **Grace, N. F.,** "Strengthening of Negative Moment Region of Reinforced Concrete Beams Using Carbon Fiber-Reinforced Polymer Strips", ACI Structural Journal; *Proceedings* V.98, N° 3, pp. 347-358, 2001.
6. **Ghali, A., Azarnejad, F.,** "Deflection Prediction of Members of Any Concrete Strength", ACI Structural Journal; *Proceedings* V.96, N° 5, pp. 807-816, 1999.
7. **Okeil, A. M., EI-Tawil, S., Shahawy, M.,** "Short-Term Tensile Strength of Carbon Fiber- Reinforced Polymer Laminates for Flexural Strengthening of Concrete Girders", ACI Structural Journal; *Proceedings* V.98, N° 4, pp. 470-478,2001.
8. **Palomino, J. L.,** "Creep Analysis of Reinforced Concrete Structures," TECNIA V.15; N° 2, pp. 25-37, Lima, 2005.
9. **Park, R., Paulay T.,** "Reinforced Concrete Structures"; John Wiley & Sons lnc.; New York,1975.
10. **Ross, C. A., Jerome, D. M., Tedesco, J. W., Hughes, M. L.,** "Strengthening of Reinforced Concrete Beams with ExternalIy Bonded Composite Laminates," ACI Structural Journal; *Proceedings* V.96, N° 2, pp. 212-220,1999.
11. **Saenz, L. P.,** "Discussion of "Equation for the Stress-Strain Curve of Concrete", by Prakash Desayi and S. Krishnan; ACI Journal; *Proceedings* V.61, N°. 9, pp. 1229-1235, 1964.
12. **Sika Perú** "Sistema de Refuerzo a Base de Polímeros Reforzados con fibra de Carbodur (CFRP),"; Hoja Técnica; Lima 1999.
13. **Wei, A., Saadatmanesh, H., Ehsani, M. R.,** "RC Beams Strengthened with FRP Plates. II: Analysis and Parametric Study", Journal of Structural Engineering; ASCE, *Proceedings* V.117, N°. 11, pp. 3434-3455, 1991.
14. **Yuan, Y., Marosszeky, M.,** "Analysis of Corroded Reinforced Concrete Sections for Repair", Journal of Structural Engineering; ASCE, *Proceedings* V.11 7, N° 7, pp. 2018-2034, 1991.

Correspondencia: jorge_lpt@cip.org.pe